Langmuir

Article

pubs.acs.org/Langmuir

Synthesis of Au@Ag Core–Shell Nanocubes Containing Varying Shaped Cores and Their Localized Surface Plasmon Resonances

Jianxiao Gong,[†] Fei Zhou,[‡,§] Zhiyuan Li,*[,‡] and Zhiyong Tang*[,†]

[†]Laboratory for Nanomaterials, National Center for Nanoscience and Technology, Beijing 100190, China

[‡]Laboratory of Optical Physics, Institute of Physics, Chinese Academy of Sciences, Beijing 100190, China

[§]Key Laboratory of Materials Physics, Anhui Key Laboratory of Nanomaterials and Nanotechnology, Institute of Solid State Physics, Chinese Academy of Sciences, Hefei 230031, Anhui, China

Supporting Information

ABSTRACT: We have synthesized Au@Ag core–shell nanocubes containing Au cores with varying shapes and sizes through modified seed-mediated methods. Bromide ions are found to be crucial in the epitaxial growth of Ag atoms onto Au cores and in the formation of the shell's cubic shape. The Au@Ag core–shell nanocubes exhibit very abundant and distinct localized surface plasmon resonance (LSPR) properties, which are core-shape and size-dependent. With the help of theoretical calculation, the physical origin and the resonance mode profile of each LSPR peak are identified and studied. The core–shell nanocrystals with varying shaped cores offer a new rich category for LSPR control through the plasmonic coupling effect between core and shell materials.

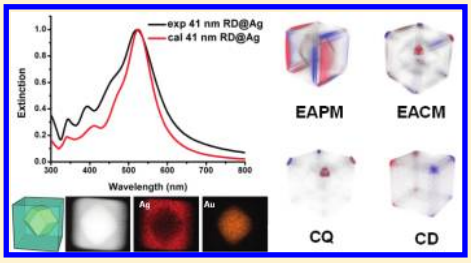

INTRODUCTION

Noble metal nanocrystals (NCs) have been one of the most rapidly developing fields in nanoscience due to distinct localized surface plasmon resonance (LSPR) and the corresponding applications in photonic devices, catalysis, biological diagnosis, recording, and therapy.[1−7] Thanks to recent progresses in both synthetic techniques and theoretical understanding, scientists are able to manipulate LSPR characteristics of noble metal NCs by changing their sizes, shapes, element species, as well as aggregation states.[6−15] Furthermore, in addition to single component, binary noble metal NCs with either core–shell or alloy structures have been extensively studied because they can offer a much broader range to tune the optical properties.[16−26] Among those, special attention has been paid to synthesize Au@Ag core–shell NCs, since Au and Ag NCs represent two types of nanomaterials that have the strongest LSPR features in visible light region.[27−31] Both sphere- and rod-shaped Au NCs have been chosen as the cores and Ag shells have been successfully coated to form core–shell structures. Experimental results demonstrate that LSPR responses of Au@Ag core–shell NCs can be tuned with the thickness of Ag shells less than 3 nm.[27] When the shell thickness exceeds a critical value of 3 nm, LSPR of the Au cores are completely screened and only the optical property of Ag shells is discerned.

We notice that current core–shell NCs are mostly prepared by homogeneous deposition of Ag shells on either Au nanorod or nanosphere cores; namely, the shortest distance at any point from the surface of cores to the surface of shells is the same. An interesting question arises: if Au NCs with different geometries are used as the cores and the thickness of Ag shells varies with the positions of Au cores, what will the optical performance of Au@Ag NCs be? To answer this question, in this work, we propose to replace conventional Au nanospheres or nanorods with the shaped Au nanopolyhedra (NPs) as the cores for fabrication of the core–shell nanostructures.

EXPERIMENTAL SECTION

Materials. Chloroauric acid tetrahydrate ($HAuCl_4·4H_2O$) and silver nitrate ($AgNO_3$) were obtained from Beijing Chemical Reagent Company. Sodium borohydride ($NaBH_4$), cetyltrimethylammonium chloride (CTAC), L-ascorbic acid (AA), and potassium bromide (KBr) were purchased from Alfa Aesar. Cetylpyridinium chloride (CPC) and cetyltrimethylammonium bromide (CTAB) were bought from Sigma Aldrich. Ultrapure water was used throughout the experiments.

Synthesis of Au NPs. Au NPs were synthesized according to our previously reported method.[12] First, the solution containing CPC capped Au spheres was made by etching and overgrowth of Au nanorods and utilized as seed solution for subsequent growth of Au NPs. Generally, 800, 200, 200, and 200 μL of CPC capped seed solution were added to 5 mL of growth solution for synthesis of 41 nm rhombic dodecahedron (RD), 73 nm RD, 72 nm octahedron, and 79 nm cube, respectively. All Au NPs were washed with 20 mM CTAC for three times and were finally dispersed in ultrapure water ([Au] = 0.8 mM) as the seed solution for preparation of Au@Ag nanocubes.

Synthesis of Au@Ag Nanocubes. Typically, 200 μL seed solution and 50 μL of 10 mM KBr was added to 5 mL of 20 mM CTAC solution and mixed, and then the solution was heated at 60 °C for 10 min. Next, 50 μL of 10 mM $AgNO_3$ and 150 μL of 100 mM AA were added. The solution was left undisturbed at 60 °C for 6 h and

Special Issue: Colloidal Nanoplasmonics

Received: November 28, 2011
Revised: February 2, 2012
Published: February 3, 2012

   dx.doi.org/10.1021/la204684u | Langmuir 2012, 28, 8959–8964

centrifuged (10 000 rpm × 10 min) two times for further characterization.

For size tuning, 800, 400, 200, 150, 100, and 50 μL seed solutions of 41 nm RDs were added while other conditions were kept constant. Control experiments were done in the absence of KBr and replacing CTAC with CTAB to examine the effect of Br^- ions in the growth process.

Characterization. Hitachi S-4800 instrument was used to record the scanning electron microscopy (SEM) images under an accelerating voltage of 10 kV. Transmission electron microscopy (TEM), scanning transmission electron microscopy (STEM), and corresponding element analysis mapping were obtained on Tecnai G2 20 S-TWIN and Tecnai G2 F20 U-TWIN under the accelerating voltage of 200 KV, respectively. UV−vis spectra were taken on a Hitachi U-3010 UV−vis spectrophotometer.

RESULTS AND DISCUSSION

Three types of different shaped Au NPs, RD with the edge length of ∼73 nm, octahedron with the edge length of ∼72 nm, and cube of the edge length of ∼79 nm, were synthesized according to our previous work (Figure S1 in the Supporting Information).[12] Note that all three-types of Au NPs had identical sizes with narrow size distributions (less than ±5%). In order to study the size effect, Au RDs with small edge length of ∼41 nm were also synthesized (Figure S1A). Subsequently, Ag shells were grown on the surface of the synthesized Au NP cores to form core−shell nanostructures. Following the published recipes,[27] we first tried to use CTAC as the surfactant to prepare core−shell NCs. However, the homogeneous nucleation of silver NCs in the growth solution was found to be serious and the morphology of the products was hard to control. The possible cause was the lower surface energy of Au NPs used in the work compared to small Au nanorods (61.7 nm × 13.5 nm,[28] and 19.8 nm × 38.3 nm[30]) and nanospheres (11 nm[27]), which made heterogeneous deposition of Ag shells onto Au NPs difficult.

Br^- ions are well-known to play an important role in promoting nucleation and growth of Ag on the Au surface through a proposed mechanism that Ag^+ ions absorb onto the facets of Au NPs in the form of AgBr.[27,30] Similar attempts were made in our experiments. However, we found that simple change of surfactants from CTAC to CTAB could not give rise to production of core−shell NCs with well-defined shapes (Figure S2). When $AgNO_3$ was added into the CTAB solution, the superfluous Br^- ions from CTAB led to formation of a large amount of AgBr, and thus AgBr precipitated accompanying with generation of polydispersed NCs (Figure S2). An alternative method adopted in our work is to introduce appropriate amount of Br^- ions into the growth solution containing CTAC to control the morphology and structure of the products (see Experimental Section). Figure 1A and B show typical large-scale SEM and TEM images of the prepared NCs of 41 nm Au RD cores and Ag shells. Remarkably, the prepared NCs have monodisperse cubic shapes with the average size of 67 nm × 67 nm × 78 nm, and the size distribution is less than 10% (Table S1). We noticed that the NCs are a little elongated, which should be due to the elongated profile of the Au RD cores. The elemental mapping further reveals that single NC is composed of Au core and Ag shell (Figure 1C). The Au RD core has the edge length of 41 nm, and the thickness of Ag shell is not uniform, in which the thickness is ∼2.8 nm at the face center (line ab in Figure 1C) and ∼20.5 nm (line cd in Figure 1C) at the corner, respectively. By altering the amount of seeds added (see Experimental Section), we obtained Au@Ag nanocubes of different sizes. The size of the core−shell NCs could be continuously tuned from ∼65 to ∼100 nm with decreasing the amount of Au NP seeds in the solution (Figure 1E−I). When more than 400 μL of seed solution was added, the shape was not able to grow to cube, as there were no sufficient Ag precursors and only a thin layer of Ag with the thickness of ∼1.5 nm was deposited on the surface of Au NPs (Figure 1D).

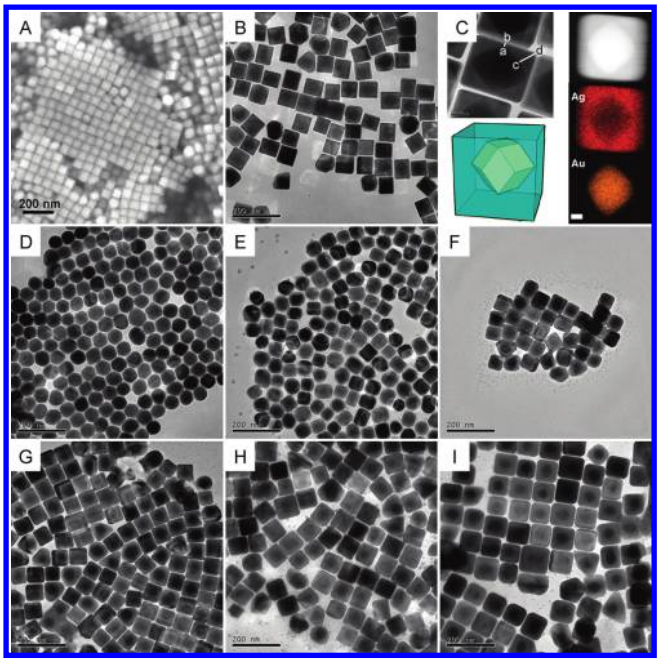

Figure 1. (A) SEM image of Au@Ag nanocubes containing 41 nm Au RD cores. (B) TEM image of Au@Ag nanocubes containing 41 nm Au RD cores. (C) STEM element analysis (right), TEM image (left-up), and sketch map (left-below) of individual Au@Ag nanocube containing 41 nm Au RD cores. (D−I) TEM images of Au@Ag NCs grown with different amounts of solution containing 41 nm Au RD seeds: (D) 800 μL, (E) 400 μL, (F) 200 μL, (G) 150 μL, (H) 100 μL, (I) 50 μL. Scale bar in (C): 10 nm.

The uniform size and shape of the Au@Ag NCs and the ability to control the thickness of the shell allow us to investigate the influence of shell and core on the LSPR property. The black curve in Figure 2A represents UV−vis spectra of as-synthesized Au@Ag nanocubes with the average size of 67 nm ×67 nm ×78 nm (samples in Figure 1A-1C) in aqueous suspension. The Au RD cores with the edge length of 41 nm exhibit a single peak at 576 nm in the UV−vis spectrum (Figure S1A). After coating with Ag shell, the LSPR peaks show tremendous change. Four new peaks emerge at 344 nm, 395 nm, 460 and 521 nm, respectively. To our best knowledge, this is the first time that so abundant and distinct LSPR features are observed for core−shell systems. To identify the physical origin of these peaks and see how the Au cores influence the LSPR performances, theoretical calculations were carried out using the discrete dipole approximation (DDA) methods.[32] In all simulations, the interdipole spacing was approximately 1 nm. Two structural modes were constructed for comparison, one of which was the Au@Ag nanocubes and the other was pure Ag nanocubes with identical sizes (see the detailed DDA calculation in the Supporting Information). The result is shown in Figure 2A and Figure S4A, respectively. Evidently, the experiment result is coincident with the calculated one.

dx.doi.org/10.1021/la204684u | Langmuir 2012, 28, 8959−8964

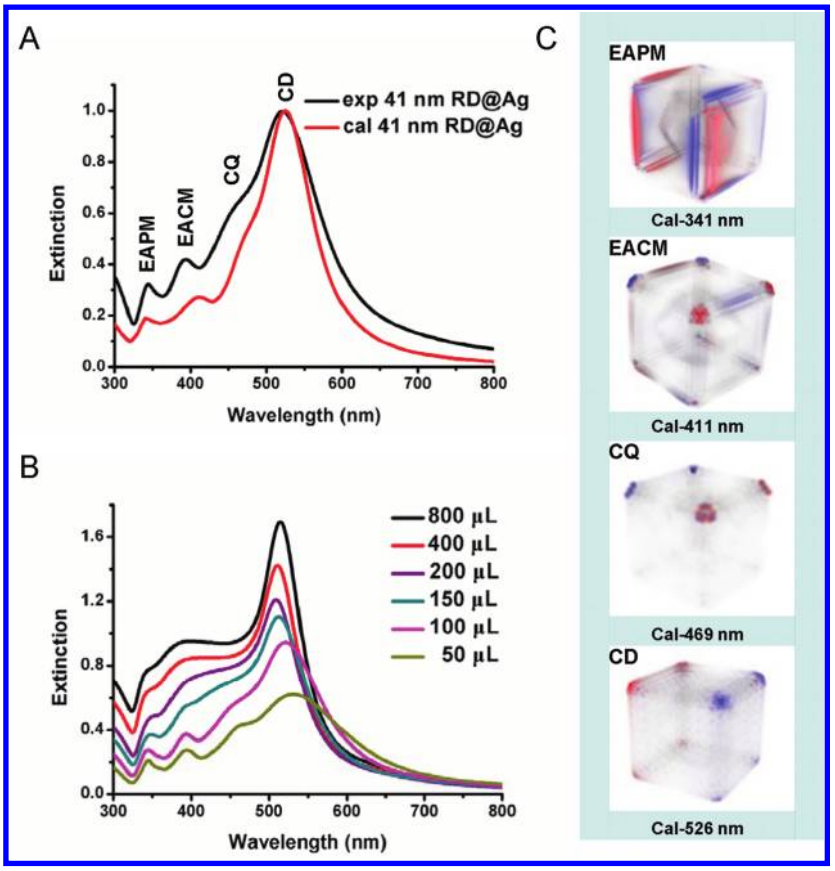

Figure 2. (A) Experimental (black) and calculated (red) extinction spectra of Au@Ag nanocubes containing 41 nm Au RD cores. (B) Experimental extinction spectra of Au@Ag NCs grown with different amounts of solution containing 41 nm Au RD seeds. The illustration number corresponds to the volume of seed solution. (C) Calculated 3D resonance maps of charge distribution under corresponding LSPR modes (identified by cal-341 nm, cal-411 nm, cal-469 nm, and cal-526 nm) of Au@Ag nanocubes containing 41 nm Au RD cores. Blue and red colors correspond to positive and negative charges, respectively, while the shade of color represents the charge density. EAPM, EACM, CQ, and CD correspond to edge associated plane multipole mode, edge associated corner multipole mode, corner quadrupole mode, and corner dipole mode, respectively.

To further distinguish each peak mode of the hybrid core−shell NCs in a visual way, the calculated three-dimensional (3D) resonance maps of polarization charge distribution are illustrated in Figure 2C. As for the Au@Ag nanocubes, the cal-341 nm peak (corresponding to exp-344 nm) is identified as edge associated plane multipole mode (EAPM mode), the cal-411 nm peak (corresponding to exp-395 nm) is recognized as edge associated corner multipole mode (EACM mode), the cal-469 nm peak (corresponding to exp-460 nm) is assigned as corner quadrupole mode (CQ mode), and the cal-526 nm peak (corresponding to exp-521 nm) is attributed as corner dipole mode (CD mode). By comparing the calculated spectrum of Au@Ag nanocubes with pure Ag nanocubes (Figure S4A), one can see that though the overall spectrum profiles are similar, there are clear peak shifts and different modes show different shift trend. The EAPM and EACM modes exhibit blue shift while the CQ and CD modes show red shift, indicating that the LSPR performance of the Au@Ag nanocubes is the coresonance effect of Au core and Ag shell rather than the mono effect of Ag shell or the simple plus of Au NC and Ag NC. According to previously reported results, when the shell of Au@Ag NCs is thicker than 3 nm, LSPR should dominantly originate from shell's contribution, as all external electromagnetic (EM) fields are screened from the core.[27] This coresonance effect should be due to the nonuniformity of the shell thickness. TEM image (Figure 1C) demonstrates the corner of Au RD core nearly touches the out facet of the Ag shell and the smallest shell thickness is around 2.8 nm, so that the EM field can penetrate the Ag shell and induces response of Au core, leading to the optical coupling between core and shell. The theoretical analysis from 3D resonance maps (Figure 2C) also supports this conclusion with the obvious charge distribution on the Au cores.

By varying the amount of seed solution added, the shell thickness and shape continuously change (Figure 1D−I), resulting in tunable LSPR properties of the core−shell NCs (Figure 2B). Even when the thinnest shell (~1.5 nm) is formed on the surface of Au RD NP (Figure 1D), the Au−Ag coresonance state is very distinct (black curve in Figure 2B). Subsequently, the resonance intensity decreases and the maximum of the main peak undergoes bathochromic shift as the shell thickness increases (black → red → purple → cyan → pink → yellow-green curves). Interestingly, the EAPM mode at around 338−345 nm switches from red shift to blue shift with an increase of the shell thickness, and the longest wavelength is obtained with Au@Ag NCs of the 200 μL seed solution case (Figure 1F and purple curve in Figure 2C). This is probably due to a new mode splitting from the original plane dipole mode as the size increases, and the detailed investigation is underway.

The shape of Au cores was altered from 41 nm RD to octahedron, cube, and RD with similar edge lengths of 72−79 nm to investigate the effect of both shape and size of Au cores on LSPR responses of core−shell NCs. Figure 3A−Cs show

dx.doi.org/10.1021/la204684u | Langmuir 2012, 28, 8959−8964

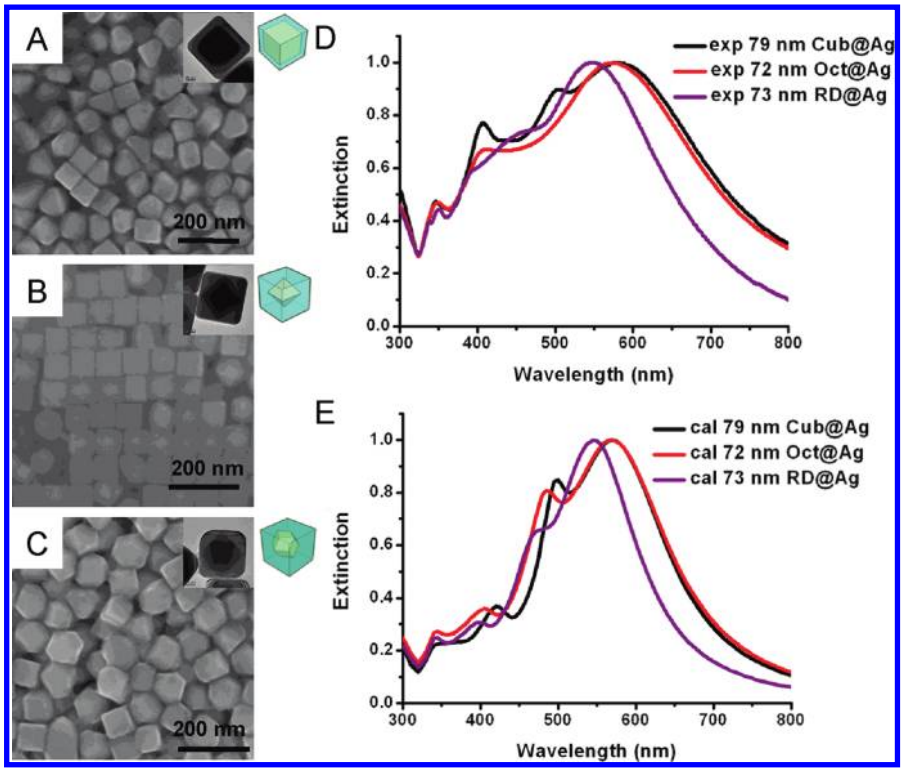

Figure 3. SEM images (A–C) and extinction spectra (D, E) of Au@Ag nanocubes containing 79 nm Au cube cores (A and black curves), Au@Ag nanocubes containing 72 nm Au octahedron cores (B and red curves), and Au@Ag nanocubes containing 73 nm Au RD cores (C and purple curves). (D) and (E) are experimental and calculated results, respectively.

SEM images of the obtained Au@Ag nanocubes after coating with Ag shells. All three samples have cubic shapes and similar edge lengths, 99 nm for Au@Ag nanocubes containing Au nanocube cores with edge length of 79 nm (Figure 3A), 98 nm for Au@Ag nanocubes containing Au octahedron cores with edge length of 72 nm (Figure 3B), and 95 nm for Au@Ag nanocubes containing Au RD cores with edge length of 73 nm (Figure 3C). It needs to be pointed out that, compared with the products in high purity prepared with 41 nm Au RD cores (Figure 1), there are some byproducts (~20%) coexisting in these samples. It is known that 12 surfaces of Au RDs are all (110) planes, whereas the surfaces of Au cubes and Au octahedra are (100) and (111) planes, respectively. Compared with the (100) and (111) planes, the (110) plane is the high energy surface for Au crystal. Therefore, Ag atoms are easily deposited onto the Au cores with (110) surfaces to form perfect core–shell structures. For RDs of different sizes, small RDs have higher surface energy than big ones, which leads to easier Ag overgrowth onto small Au RDs compared with big Au RDs. These causes are why byproducts appear in Figure 3.

The LSPR properties of Au@Ag nanocubes containing Au cores with varying shapes and sizes are shown in Figure 3D, with the calculated results shown in Figure 3E. The overall agreement between experiment and theory is pretty good in regard to the number, the position and the relative intensity of most LSPR peaks. However, there are some certain mismatches in the line shape (e.g., the width) of peaks between experimental and theoretical results, which most likely originate from the byproducts in the samples. From the simulation curves (Figure S4B–S4D), one can see similar shift trend of the LSPR peaks of the core–shell nanocubes compared with the reference pure Ag nanocubes with similar sizes except for Au@Ag nanocubes containing Au cube cores (Figure S4B); that is, two peaks at the long wavelengths (CQ and CD modes) red shift whereas another two peaks at the short wavelengths (EAPM and EACM modes) blue shift. This difference in optical performances lies in the fact that the shell thickness of the Au@Ag nanocubes containing Au cube cores is uniform and exceeds 3 nm, while shells in other Au@Ag nanocubes are nonuniform. The uniform shell of the Au@Ag nanocubes containing Au cube cores completely screens external EM fields against Au cores. Furthermore, by changing the core shapes, the LSPR modes are tuned both in position and resonance mode profile (see Figure S3 for 3D resonance maps and Figure S4 for spectra). All the above results highlight the importance of the shape and size of Au cores on the overall optical performances of Au@Ag NCs.

It should be stressed out that, in addition to the usual routes to control LSPR in solid NCs by means of their sizes and shapes, the current Au@Ag NCs with varying core sizes and shapes offer another big class of methods to manipulate LSPR by making use of the core–shell plasmonic coupling effect. As the inner cores and outer shells both can have many geometric freedoms, their combination yields a much richer category of the overall core–shell NC morphologies that can be fully harnessed to realize a wide variety of LSPR properties for applications in various areas such as optical sensing, fluorescence imaging, surface enhanced Raman scattering, biological diagnosis, and therapy.

■ CONCLUSIONS

In conclusion, we have synthesized Au@Ag core–shell nanocubes containing Au cores with varying shapes and sizes. Through forming a complex with Ag^+ ions, bromide ions are crucial for the epitaxial growth of Ag shells onto the surface of

dx.doi.org/10.1021/la204684u | *Langmuir* 2012, 28, 8959–8964

Au surfaces. For the first time, we obtained Au@Ag core−shell NCs with very abundant and distinct LSPR characteristics. Theoretical calculations clearly reveal that such unique LSPR properties originate from strong electromagnetic coupling between Au cores and Ag shells. The LSPR responses of the Au@Ag core−shell NCs show core-shape and core-size dependence, which will greatly enrich the manipulation of optical properties of NCs not only by means of the size and shape of core and shell materials alone, but also by making use of the plasmonic coupling effect between cores and shells.

■ ASSOCIATED CONTENT

Supporting Information

Geometrical mode for discrete dipole approximation (DDA) simulation, calculation of charge distribution, SEM images and UV−vis spectra of Au cores, SEM images of samples synthesized with CTAB and without KBr, calculated 3D resonance maps of polarization charge distribution for Au@Ag NCs with different shaped cores, and calculated extinction spectra of core−shell and pure Ag nanocubes. This material is available free of charge via the Internet at http://pubs.acs.org.

■ AUTHOR INFORMATION

Corresponding Author

*E-mail: zytang@nanoctr.cn (Z.Y.T.); lizy@aphy.iphy.ac.cn (Z.Y.L.).

Notes

The authors declare no competing financial interest.

■ ACKNOWLEDGMENTS

This work was supported by the National Natural Science Foundation for Distinguished Youth Scholars of China (21025310, Z.Y.T.), China-Korea Joint Research Project (2010DFA51700, Z.Y.T.), 100-Talent Program of Chinese Academy of Sciences (Z.Y.T.), the National Natural Science Foundation of China (60736041 and 10874238, Z.Y.L.), and the Knowledge Innovation Program of the Chinese Academy of Sciences (Y1 V2013L11, Z.Y.L.).

■ REFERENCES

(1) Tao, A.; Sinsermsuksakul, P.; Yang, P. Polyhedral Silver Nanocrystals with Distinct Scattering Signatures. *Angew. Chem., Int. Ed.* **2006**, *45*, 4597−4601.

(2) Huang, H.; Yu, C.; Chang, H.; Chiu, K.; Chen, H.; Liu, R.; Tsai, D. Plasmonic optical properties of a single gold nano-Rod. *Opt. Express* **2007**, *15*, 7132−7139.

(3) Pyayt, A. L.; Wiley, B.; Xia, Y.; Chen, A.; Dalton, L. Integration of photonic and silver nanowire plasmonic waveguides. *Nat. Nanotechnol.* **2008**, *3*, 660−665.

(4) Cao, Y. C.; Jin, R.; Mirkin, C. A. Nanoparticles with Raman spectroscopic fingerprints for DNA and RNA detection. *Science* **2002**, *297*, 1536−1540.

(5) Mulvihill, M. J.; Ling, X. Y.; Henzie, J.; Yang, P. Anisotropic etching of silver nanoparticles for plasmonic structures capable of single-particle SERS. *J. Am. Chem. Soc.* **2009**, *132*, 268−274.

(6) Sorrell, C. D.; Carter, M. C. D.; Serpe, M. J. Color Tunable Poly (*N*-Isopropylacrylamide)-*co*-Acrylic Acid Microgel-Au Hybrid Assemblies. *Adv. Funct. Mater.* **2011**, *21*, 425−433.

(7) Zijlstra, P.; Chon, J. W. M.; Gu, M. Five-Dimensional optical recording mediated by surface plasmons in gold nanorods. *Nature* **2009**, *459*, 410−413.

(8) Sun, Y.; Xia, Y. Shape-Controlled synthesis of gold and silver nanoparticles. *Science* **2002**, *298*, 2176−2179.

(9) Jin, R.; Charles Cao, Y.; Hao, E.; Metraux, G. S.; Schatz, G. C.; Mirkin, C. A. Controlling anisotropic nanoparticle growth through plasmon excitation. *Nature* **2003**, *425*, 487−490.

(10) Noguez, C. Surface plasmons on metal nanoparticles: the influence of shape and physical environment. *J. Phys. Chem. C* **2007**, *111*, 3806−3819.

(11) Seo, D.; Yoo, C. I.; Park, J. C.; Park, S. M.; Ryu, S.; Song, H. Directed surface overgrowth and morphology control of polyhedral gold nanocrystals. *Angew. Chem., Int. Ed.* **2008**, *120*, 775−779.

(12) Niu, W.; Zheng, S.; Wang, D.; Liu, X.; Li, H.; Han, S.; Chen, J.; Tang, Z.; Xu, G. Selective synthesis of single-Crystalline rhombic dodecahedral, octahedral, and cubic gold nanocrystals. *J. Am. Chem. Soc.* **2008**, *131*, 697−703.

(13) Zhang, Q.; Hu, Y.; Guo, S.; Goebl, J.; Yin, Y. Seeded growth of uniform Ag nanoplates with high aspect ratio and widely tunable surface plasmon bands. *Nano Lett.* **2010**, *10*, 5037−5042.

(14) Haynes, C. L.; McFarland, A. D.; Zhao, L. L.; Van Duyne, R. P.; Schatz, G. C.; Gunnarsson, L.; Prikulis, J.; Kasemo, B.; Kall, M. Nanoparticle Optics: the Importance of Radiative Dipole Coupling in Two-Dimensional Nanoparticle Arrays. *J. Phys. Chem. B* **2003**, *107*, 7337−7342.

(15) Huang, X.; Tang, S.; Mu, X.; Dai, Y.; Chen, G.; Zhou, Z.; Ruan, F.; Yang, Z.; Zheng, N. Freestanding palladium nanosheets with plasmonic and catalytic properties. *Nat. Nano.* **2011**, *6*, 28−32.

(16) Fan, F. R.; Liu, D. Y.; Wu, Y. F.; Duan, S.; Xie, Z. X.; Jiang, Z. Y.; Tian, Z. Q. Epitaxial Growth of Heterogeneous Metal Nanocrystals: From Gold Nano-Octahedra to Palladium and Silver Nanocubes. *J. Am. Chem. Soc.* **2008**, *130*, 6949−6951.

(17) Habas, S. E.; Lee, H.; Radmilovic, V.; Somorjai, G. A.; Yang, P. Shaping binary metal nanocrystals through epitaxial seeded growth. *Nat. Mater.* **2007**, *6*, 692−697.

(18) Grzelczak, M.; Rodríguez-González, B.; Pérez-Juste, J.; Liz-Marzán, L. M. Quasi-Epitaxial Growth of Ni Nanoshells on Au Nanorods. *Adv. Mater.* **2007**, *19*, 2262−2266.

(19) Lee, H.; Habas, S. E.; Somorjai, G. A.; Yang, P. Localized Pd overgrowth on cubic Pt nanocrystals for enhanced electrocatalytic oxidation of formic acid. *J. Am. Chem. Soc.* **2008**, *130*, 5406−5407.

(20) Mazumder, V.; Chi, M.; More, K. L.; Sun, S. Core/shell Pd/FePt nanoparticles as an active and durable catalyst for the oxygen reduction reaction. *J. Am. Chem. Soc.* **2010**, *132*, 7848−7849.

(21) Yu, Y.; Zhang, Q.; Liu, B.; Lee, J. Y. Synthesis of Nanocrystals with Variable High-Index Pd Facets through the Controlled Heteroepitaxial Growth of Trisoctahedral Au Templates. *J. Am. Chem. Soc.* **2010**, *132*, 18258−18265.

(22) Tedsree, K.; Li, T.; Jones, S.; Chan, C. W. A.; Yu, K. M. K.; Bagot, P. A. J.; Marquis, E. A.; Smith, G. D. W.; Tsang, S. C. E. Hydrogen production from formic acid decomposition at room temperature using a Ag-Pd core-Shell nanocatalyst. *Nat. Nanotechnol.* **2011**, *6*, 302−307.

(23) Cortie, M. B.; McDonagh, A. M. Synthesis and Optical Properties of Hybrid and Alloy Plasmonic Nanoparticles. *Chem. Rev.* **2011**, *111*, 3713−3735.

(24) Zhang, H.; Jin, M.; Wang, J.; Li, W.; Camargo, P. H. C.; Kim, M. J.; Yang, D.; Xie, Z.; Xia, Y. Synthesis of Pd-Pt Bimetallic Nanocrystals with a Concave Structure through a Bromide-Induced Galvanic Replacement Reaction. *J. Am. Chem. Soc.* **2011**, *133*, 6078−6089.

(25) Lim, B.; Kobayashi, H.; Yu, T.; Wang, J.; Kim, M. J.; Li, Z.-Y.; Rycenga, M.; Xia, Y. Synthesis of Pd-Au Bimetallic Nanocrystals via Controlled Overgrowth. *J. Am. Chem. Soc.* **2010**, *132*, 2506−2507.

(26) Lu, C. L.; Prasad, K. S.; Wu, H. L.; Ho, J. A.; Huang, M. H. Au nanocube-directed fabrication of Au-Pd core-shell nanocrystals with tetrahexahedral, concave octahedral, and octahedral structures and their electrocatalytic activity. *J. Am. Chem. Soc.* **2010**, *132*, 14546−14553.

(27) Ma, Y.; Li, W.; Cho, E. C.; Li, Z.; Yu, T.; Zeng, J.; Xie, Z.; Xia, Y. Au@Ag Core-Shell Nanocubes with Finely Tuned and Well-Controlled Sizes, Shell Thicknesses, and Optical Properties. *ACS Nano* **2010**, *4*, 6725−6734.

(28) Sánchez-Iglesias, A.; Carbó-Argibay, E.; Glaria, A.; Rodríguez-González, B.; Pérez-Juste, J.; Pastoriza-Santos, I.; Liz-Marzán, L. M. Rapid Epitaxial Growth of Ag on Au Nanoparticles: From Au Nanorods to Core-Shell Au@ Ag Octahedrons. *Chem.—Eur. J.* **2010**, *16*, 5558−5563.
(29) Liu, M.; Guyot-Sionnest, P. Synthesis and optical characterization of Au/Ag core/shell Nanorods. *J. Phys. Chem. B* **2004**, *108*, 5882−5888.
(30) Cho, E. C.; Camargo, P. H. C.; Xia, Y. Synthesis and Characterization of Noble-Metal Nanostructures Containing Gold Nanorods in the Center. *Adv. Mater.* **2010**, *22*, 744−748.
(31) Park, G.; Seo, D.; Jung, J.; Ryu, S.; Song, H. Shape Evolution and Gram-Scale Synthesis of Gold@Silver Core-Shell Nanopolyhedrons. *J. Phys. Chem. C* **2011**, *115*, 9417−9423.
(32) Zhou, F.; Li, Z. Y.; Liu, Y.; Xia, Y. Quantitative Analysis of Dipole and Quadrupole Excitation in the Surface Plasmon Resonance of Metal Nanoparticles. *J. Phys. Chem. C* **2008**, *112*, 20233−20240.